Preliminary Study of the Behavior of Composite Material Box Beams Subjected to Impact

Jason R. Smith, Lawrence C. Bank[1], and **Michael E. Plesha**

Engineering Mechanics and Astronautics Program
Department of Engineering Physics
and
Department of Civil and Environmental Engineering
University of Wisconsin-Madison
Madison, WI 53706

---

[1] To whom all correspondence should be addressed. Department of Civil & Environmental Engineering, University of Wisconsin-Madison, 1415 Engineering Drive, Madison, WI 53706, USA. e-mail: bank@engr.wisc.edu

ABSTRACT

LS-DYNA 940.2 was used to study the response of composite box beams subjected to oblique (or inclined) impacts by a rigid cylinder. The square cross-section composite beams were 1000 mm long with 50 mm by 50 mm nominal cross-sectional dimensions. The rigid cylinder had a 50 mm diameter and a 100 mm length and impacted the box beam on the top panel. The composite box beam and the cylinder were modeled with 3 mm thick Belytschko-Tsay shell elements. Material 54: MAT_ENHANCED_COMPOSITE_DAMAGE was used to model the orthotropic composite material used in the sidewalls of the box beam. In order to simulate an experimentally observed progressive "tearing" failure in the box beams during the impact events, spotwelds were used to model the corners of the beams (i.e. the joints between the four sides of the box beam). Spotweld failure parameters were calculated from the transverse tensile and in-plane shear strengths of the composite material. The benchmark analysis used for the study was one in which the rigid cylinder hit the beam at an incident angle of 25° to the horizontal axis at a velocity of 2 m/s. The coefficient of friction between the cylinder and the beam was 0.1. The results of the benchmark analysis were compared to results of analyses with various angles of impact, impact velocities, and coefficients of friction. Results were compared with respect to the displacement path of the cylinder, the angle of the path of the cylinder with respect to the horizontal direction (rebound angle), the change in velocity of the cylinder, and the resultant impact force on the cylinder. In general, the rebound angle and velocity of the cylinder appeared to have a rational dependence on the incident angle, the coefficient of friction, and the initial velocity.

INTRODUCTION

Multicellular, thin-walled, composite material beams are being considered as light-weight, economical, and enhanced energy absorbing guardrails for roadside safety applications. In prior studies the second author and co-workers have studied the response of pultruded glass-fiber reinforced polymer materials and thin-walled tubes subjected to drop weight impacts (Svenson et al., 1993, 1995). In these preliminary experimental studies, the objective was to gain an understanding of the energy absorbing mechanisms and failure characteristics of pultruded composite materials reinforced by multifilament rovings and continuous strand mats. In further tests on pultruded single-cell tubes (Palmer et al., 1997, 1998) and on multicellular tubes (Gentry et al., 1996), a typical and beneficial progressive failure mechanism in pultruded tubes, called a "tearing" failure mechanism, was observed. In this mechanism, the pultruded tube, which has a high proportion of longitudinal rovings and only a small proportion of continuous mats, tends to fail progressively by splitting along the corners of the tube when subjected to transverse impact loads. Figure 1 shows a close up of the failure of a prototype multicellular composite material guardrail following transverse impact by an 800 kg pendulum at 35 km/h.

Early attempts to use LS-DYNA to model this progressive tearing failure are described in Palmer et al. (1997, 1998). In these studies, LS-DYNA was used to develop simulations of quasi-static, displacement-controlled tests of single-cell pultruded tubes. Load was applied to the composite thin-walled beam using a rigid cylinder with a prescribed constant velocity. Spotwelds were used as connections at the corners of the tubes. In these simulations, the loading head speeds were many orders of magnitude faster than in the static tests; nevertheless, the results were reasonably satisfactory. The progressive tearing failure was reasonably well captured by progressive failure of spotwelds at the corners of the beams. Simulations of multicelled composite guardrail prototypes subjected to pendulum impact tests at the US Federal Highway Administration are reported on by Gentry and Bank (2000). Once again spotwelds were used as connections at the corners of the multiple tubular sections used in the guardrail beams.

Figure 1. Post Impact Photograph of Multicellular Composite Guardrail Showing "Tearing."

Results of the simulations were again "reasonable," with most disagreement between the experimental and simulated impact test results coming from the fact that spotwelds tended to "unzip" too quickly in the initial stages of the simulation. This caused the system to lose stiffness too quickly.

In all the prior work described above, the impactor has always been deployed perpendicular to the beam, either with constant velocity or with an initial velocity. In actual crash testing, the impacting vehicle is deployed at varying incident angles to the beam and at varying velocities. Of interest in a vehicular crash test of this type is the eventual path and velocity of the vehicle as it exits the guardrail system (NCHRP 350, 1993). In order to develop an understanding of the key parameters needed for simulating an inclined impact with a multicellular composite material guardrail, a preliminary study was conducted on the response of a single-cell thin-walled pultruded box beam, subjected to inclined impacts. The long-term objective of the study was to provide data for the optimal design of thin-walled pultruded tubes that would cause the cylinder to rebound with the lowest possible exit angle and velocity. The study was also done to provide design input for testing individual tubes with semi-rigid end-conditions that are currently underway. The details of the simulation study are reported in this paper.

LS-DYNA MODEL

The finite element model of the inclined impact test used in the LS-DYNA simulations is shown in Figure 2. The "box beam" was modeled as four separate plates that were attached together using spotwelds. The ends of all the plates were fully restrained so as to represent a fixed-fixed beam. The beam was impacted at the third-point of its span by a cylindrical impactor that was given an initial velocity and an initial incident angle relative to the beam. The cylinder was constrained to move in the plane of the beam throughout its motion in order to prevent undesired twisting following impact.

The beam was modeled with 1280 three-mm thick Belytschko-Tsay shell elements using material 54 (MAT_ENHANCED_COMPOSITE_DAMAGE) with the Chang and Chang

failure criterion. The material properties used for the pultruded fiber composite material are given in Table 1. Default values were used for all other material model variables. Eight through the thickness integration points were used for the shell elements in the beam. The cylinder was modeled with 3 mm thick Belytschko-Tsay shell elements using material 20 (MAT_ RIGID). In order to obtain a cylinder mass of 55.4 kg, which was similar to that used in drop weight experiments (Svenson et al., 1995), the density of the cylinder was taken as 150 times the density of steel. The Young's modulus and Poisson ratio of the cylinder were those of steel.

The vertical sides of the tube were offset 3 mm from the horizontal sides and "spotwelds" (CONSTRAINED_SPOTWELD) were used to connect the nodes of the vertical and horizontal sides. The normal and shear strengths for the spotwelds were calculated from the transverse tensile strength (YT) and the in-plane shear strength (SC) for the composite material shown in Table 1, the wall thickness (3 mm), and the distance between the nodes (6.25 mm). To account for the reduced strength of the composite material at the corners, the material strengths were reduced by 50% giving SN = 450 N and SS = 646.9 N, which are the normal and shear forces at spotweld failure respectively. The spotweld failure criterion exponents, M for the shear spotweld force and N for the normal spotweld force, were both taken as 1.0.

Automatic contact (CONTACT_AUTOMATIC_SURFACE_TO_SURFACE) between surfaces was used for contact between the cylinder and all the sides of the box beam and for contact between the sides themselves. A functional coefficient of friction of 0.1 was used for all contact surfaces. It only changed for the contact surfaces between the cylinder and the box beam when this parameter was under investigation. Hourglass control was accomplished using the stiffness form with an hourglass coefficient of 0.05.

Computations were performed on a Pentium II 450 MHz machine with 384 MB RAM under Windows NT running the NT version of LS-DYNA 940.2 supplied by KBS2.

PARAMETRIC STUDIES

Parametric studies were conducted. The key variables were the incident angle, the impact velocity, and the coefficient of friction. The "benchmark" analysis consisted of an impact with an incident angle of 25° at 2 m/s with a coefficient of friction of 0.1. Parameters included incident angles of 25°, 40°, and 55°, impact velocities of 2, 3, and 5 m/s and coefficients of friction of 0.1, 0.25, and 0.5.

ANALYSIS OF RESULTS

The results of the LS-DYNA simulations were analyzed both qualitatively and quantitatively. Qualitatively, the simulations were analyzed to determine if the progressive failure of the spotwelds at the corners of the box beams was occurring as desired. The nature of the failure mode of the sidewalls of the beam and the trajectory of the cylinder following impact was also studied qualitatively from the animation plots. Quantitative analysis consisted of displacement (δ), velocity (v), and acceleration (a) data obtained from the cylinder, energy data from the system and from the parts, and derivatives of this data such as resultant velocity at exit, exit angle at rebound, and impact force on the cylinder. The mass of the cylinder ($m_{cylinder}$) was used in the calculation of the impact force. As noted previously, the rebound velocity and angle are used in the evaluation of vehicle crash tests. The following equations were used to calculate the inclination of the cylinder to the horizontal ($\theta_{cylinder}$), the resultant velocity ($v_{resultant}$) of the cylinder, and the resultant force on the cylinder ($F_{resultant}$):

$$\theta_{cylinder} = \tan^{-1}(\delta_z / \delta_x) = \tan^{-1}(\delta_{vertical} / \delta_{horizontal}) \tag{1}$$

$$v_{resultant} = \sqrt{(v_x^2 + v_z^2)} = \sqrt{(v_{horizontal}^2 + v_{vertical}^2)} \tag{2}$$

$$F = m_{cylinder} \cdot a_{cylinder} \tag{3}$$

$$F_{resultant} = \sqrt{(F_x^2 + F_z^2)} = \sqrt{(F_{horizontal}^2 + F_{vertical}^2)} \tag{4}$$

All acceleration data used to calculate the force on the cylinder was filtered according to the SAE filter technique (SAE Recommended Practice, 1995). The upper cut-off frequency, based on the fundamental frequency of flexural vibration of the fixed-fixed beam, was 235 Hz.

In the results that follow, the data has been represented in a number of different forms to assist in interpretation. To represent the trajectory of the cylinder, the "displacement path" of the cylinder has been plotted with respect to the horizontal axis. In these plots (Figs. 4, 8, and 12), the initial position of the upper, outer surface of the beam prior to impact is represented as a dashed line at -7 mm of vertical displacement. The path of the cylinder as it travels downward and along the beam is shown. The path is a function of the local damage due to the impact and the beam flexural deformation. The path is shown for a reference point at the bottom of the cylinder that initially contacts the beam. Since the cylinder is restrained to move only in the X-Z plane and not to rotate about its own axis, this point remains at the bottom of the cylinder throughout the simulation. The trajectory of the cylinder is also represented in "angle to horizontal" plots. In these plots (Figs. 5, 9, and 13), the angle to the horizontal of the reference point is plotted as a function of time. The incident angle is shown as a negative angle on the left hand side, while the exit angle at rebound (if it occurs) is shown as a positive angle on the right hand side of the plot. The change in velocity of the cylinder during the impact is shown in "resultant velocity" plots (Figs. 6, 10, and 14). The velocity of the cylinder as a function of time is shown for the reference point. The decrease in the resultant velocity of the cylinder as it travels along the beam and subsequently rebounds is directly related to the kinetic energy of the cylinder. A decrease in the velocity of the cylinder implies energy absorption by the composite beam during the impact event. The final set of plots is one showing "resultant force" on the cylinder (Figs. 7, 11, and 15). These plots give a measure of the duration and magnitude of the load on the beam as well as an indication of when the cylinder loses contact with the beam. Each curve of the force vs. time plots shows a peak force followed by a decrease. Sudden reductions in the force were due to several spotwelds breaking along the upper corners of the beam directly beneath the load head. Buckling of the vertical walls of the beam directly under the load head also contributed significantly to these reductions. Spotwelds continued to break progressively following this initial reduction in force, primarily along the upper corners of the beam. An example of the typical progressive spotweld failure emanating from the point of impact can be seen in Figure 3.

DISCUSSION OF RESULTS

The four forms of data were used to compare the behavior of the impacted beams subjected to different initial conditions. Analyses at different initial conditions were compared to the benchmark condition of 25°, 2 m/s, and a coefficient of friction of 0.1.

The influence of impact velocity is shown in Figures 4 to 7. For this portion of the study, all impact angles were 25° with the coefficient of friction for the contact between the cylinder and the beam given a value of 0.1. The following impact velocities were then investigated: 2

m/s, 3 m/s, and 5 m/s. Figure 4 shows that the cylinder rebounded quicker with less penetration and beam deflection as the impact velocity decreased. An impact velocity of 5 m/s caused overall flexural failure of the beam and no cylinder rebound occurred. Figure 5 demonstrates that as the impact velocity increased the angle with which the cylinder rebounded was reduced to a greater degree. The cylinder exited the 2 m/s impact at an angle of 21.5° and exited the 3 m/s impact at an angle of 18.5°. Since the 5 m/s impact never rebounded, no rebound angle was possible. Figure 6 shows that as the impact velocity increased so did the drop in velocity following impact. The following velocity changes were observed in the velocity magnitude after rebound: a 415.85 mm/s (0.416 m/s) drop for the 2 m/s impact and an 862.07 mm/s (0.862 m/s) drop for the 3 m/s impact. For the 5 m/s impact that broke through the beam, a drop of 778 mm/s (0.778 m/s) was measured. Finally, in Figure 7, we see that as the impact velocity increased the peak force occurred earlier. Hence, the spotwelds broke sooner and buckling of the sidewalls occurred earlier for faster impact velocities. Element failure also contributed to the sudden drops in the force plots at higher velocities. Spotweld failures typically occurred at the top corners of the beam, initiated under the load head, and propagated towards the beam bends. At the impact velocity of 5 m/s, the progressive spotweld failure also occurred at the bottom corners of the beam, beginning beneath the load head. This contributed to overall failure of the beam.

The influence of coefficient of friction between the cylinder and the beam is shown in Figures 8 to 11. For this portion of the study, all impact angles were 25° with an impact velocity of 2 m/s. The following coefficients of friction (μ_c) between the cylinder and the beam were then investigated: 0.1, 0.25, and 0.5. Figure 8 shows that the cylinder rebounded only slightly quicker as the coefficient of friction increased. The main difference here between the different coefficients of friction is much more apparent in the distance along the beam span that the cylinder traveled. As the coefficient of friction increased, the cylinder traveled further along the beam. Figure 9 demonstrates that the coefficient of friction had a significant effect on the angle after impact. Although the cylinder left the beam with the same angle that it entered for a coefficient of friction of 0.25, there was a change in the angle after impact for the other values investigated. The angle after impact reduced to 21.5° for the coefficient of friction of 0.1and increased to 33.5° for the coefficient of friction of 0.5. Figure 10 shows that as the coefficient of friction increased the drop in velocity following impact increased. The following velocity changes were observed: a 415.85 mm/s (0.416 m/s) drop for μ_c = 0.1, a 607.74 mm/s (0.608 m/s) drop for μ_c = 0.25, and a 918.78 mm/s (0.919 m/s) drop for μ_c = 0.5. Figure 11 shows that as the coefficient of friction increased the peak force increased. The duration of the impact event was not affected by the coefficient of friction.

The influence of incident angle is shown in Figures 12 to 15. For this portion of the study, all impact velocities were 2 m/s with a value of 0.1 for the coefficient of friction between the cylinder and the beam. The following angles of impact were then investigated: 25°, 40°, and 55°. Despite the fact that the angles of impact were different for this particular comparison, the location of first impact was still directed at a point a distance approximately 1/3 of the beam span from the nearest beam end. Figure 12 shows that the cylinder rebounded quicker and left contact with the beam after much less penetration of the beam as the angle of impact decreased. Figure 13 demonstrates that as the angle of impact increased the drop in the angle following impact was greater. The following drops were noted: the 25° impact angle reduced to 21.5° after impact, the 40° impact angle reduced to 30°, and the 55° impact angle dropped to 40.5°. Figure 14 shows that as the angle of impact increased so did the drop in velocity following impact. The following velocity changes were observed: a 415.85 mm/s (0.416 m/s) drop for the 25° impact angle, a 871.47 mm/s (0.871 m/s) drop for the 40° impact angle, and an 1133.9 mm/s (1.134 m/s) drop for the 55° impact angle. There was also a distinguishable increase in the velocity plot for the 55° impact angle following the impact (~0.035 s) which can be attributed to the beam acting as a slingshot to restore some velocity to the cylinder. In

Figure 15, it is seen that as the angle of impact increased the peak force occurred earlier and was larger. Hence, the spotwelds broke sooner for higher angles of impact and the sidewalls buckled earlier under the cylinder. A secondary contributing factor to the large, sudden drop in force for the model with the 55° impact angle was global beam failure as the majority of the elements at the beam end nearest the initial impact failed as shown in Figure 16.

Observations of the animations and energy data for the different runs revealed some inconsistencies with the simulations, which were unresolved at the time of writing. In the velocity comparisons, there were a number of problems with the output for the model run at an impact velocity of 5 m/s. There was a sudden, explosive spotweld failure encountered with this model as shown in Figure 17. This type of spotweld failure, to a lesser extent, was also seen in the models with coefficients of friction of 0.25 and 0.5. Although there were no problems encountered with the hourglassing energy (since it remained low with respect to the internal energy), there were other energy problems encountered elsewhere. There was a small dip in the total energy for the model with an impact angle of 55° and both the total and sliding interface energies were seen to suddenly drop to zero for the model with an impact velocity of 5 m/s. Generally global energy data were good as shown for the benchmark model in Figure 18.

CONCLUSIONS

The progressive failure of composite box beams subjected to oblique impacts was modeled using spotwelds to connect the sidewalls of the beams at their corners. Buckling of the vertical sidewalls near the impact contributed greatly to the desired progressive "tearing" failure of interest in this study. This progressive failure was witnessed in most of the parametric studies conducted that involved comparisons between angles of impact, impact velocities, and coefficients of friction. Element failure in the beam away from the initial impact limited the desired unzipping effect in the spotwelds as the velocity and angle of impact approached their upper limits in this study. A desirable reduction in the post-impact exit angle and in the rebound velocity was observed in most of the simulations. However, it was also noted that increased coefficients of friction were able to increase the rebound angle after impact. An attractive, gradual decrease in impact force was exhibited after the peak force was reached in all models. The results of this numerical study show that finite element modeling can serve as a valuable tool in providing both qualitative and quantitative data that can be used to optimize the design of complex composite material structures.

ACKNOWLEDGEMENTS

REFERENCES

GENTRY, T.R., BANK, L.C., YIN, J. and LAMTENZAN, J.D. (1996). "Damage Evolution and Progressive Failure in Composite Material Highway Guardrails," Crashworthiness and Occupant Protection in Transportation Systems - 1996 (eds. H.F. Mahmood and M.R. Baccouche), AMD-Vol. 218, ASME, NY, pp. 79-89.

GENTRY, T.R. and BANK, L.C. (2000). "Pendulum Impacts into FRP Composite Guardrail Prototypes: Testing and Simulation," 79th Transportation Research Board Annual Meeting, Paper no. 00-0481, Washington, DC.

NCHRP (1993). <u>Recommended Procedures for the Safety Performance Evaluation of Highway Features</u>, National Cooperative Highway Research Program Report 350, National Research Council, Washington, D.C.

PALMER, D.W., BANK, L.C. and GENTRY, T.R. (1997). "Simulation of Progressive Failure of Pultruded Composite Beams in Three Point Bending using LS-DYNA3D," in proceedings of the <u>SPI/ICE 97</u>, Nashville, TN, January 27-29, Session 14-C 1-12.

PALMER, D.W., BANK, L.C. and GENTRY, T.R. (1998). "Progressive Tearing Failure of Pultruded Composite Box Beams: Experiment and Simulation," <u>Composites Science and Technology</u>, Vol. 58, No. 8, pp. 1353-1359.

SAE Recommended Practice (1995). "Instrumentation for Impact Test – Part 1 – Electronic Instrumentation – SAE J211/1 MAR95," Society for Automotive Engineers, MI.

SVENSON, A.L., HARGRAVE, M.W., and BANK, L.C. (1993). "Impact Behavior of Pultruded Composites," in the proceedings of the <u>48th Annual SPI Conference</u>, Composites Institute, Society for the Plastics Industry, Cincinnati, OH, February 8-11, Session 21-D, pp. 1-6.

SVENSON, A.L., HARGRAVE, M.W., TABIEI, A., BANK, L.C., and TANG, Y. (1995). "Design of Pultruded Beams for Optimization of Impact Performance," in the proceedings of the <u>50th Annual SPI Conference</u>, Composites Institute, Society for the Plastics Industry, Cincinnati, OH, January 28 - February 1, Session 10-E, pp. 1-7.

Table 1. Material Properties for Composite Material in LS-DYNA models

Parameter	Description	Value
ρ (RO)	Mass density	1.939×10^{-9} kg x 10^3 / mm^3
E_a (EA)	Young's modulus – longitudinal (fiber) direction	20.69×10^3 MPa
E_b (EB)	Young's modulus – transverse direction	6.89×10^3 MPa
ν_{ba} (PRBA)	Minor Poisson's ratio	0.10
G_{ab} (GAB)	Shear modulus in plane of element	2.5×10^3 MPa
G_{bc} (GBC)	Shear modulus in normal / transverse direction	1.25×10^3 MPa
G_{ca} (GCA)	Shear modulus in normal / longitudinal direction	2.5×10^3 MPa
X_C (XC)	Longitudinal compressive strength	0.207×10^3 MPa
X_T (XT)	Longitudinal tensile strength	0.207×10^3 MPa
Y_C (YC)	Transverse compressive strength	0.103×10^3 MPa
Y_T (YT)	Transverse tensile strength	0.048×10^3 MPa
S_C (SC)	In-plane shear strength	0.069×10^3 MPa
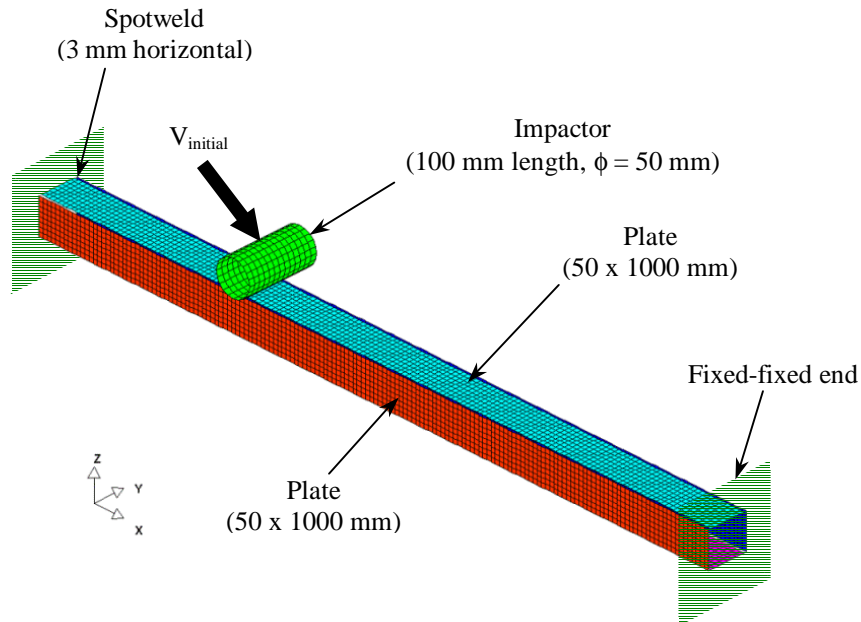
Figure 2. Isometric View of Typical LS-DYNA Model

TIME = 3.5798412E-002
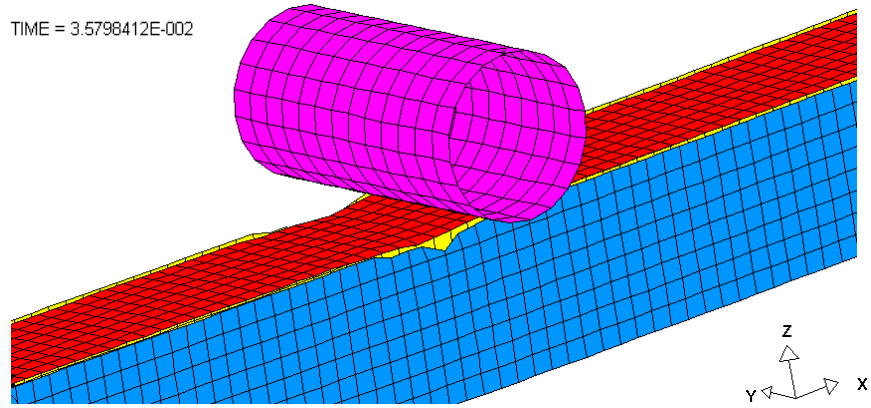
Figure 3. Displacement Animation Plots Showing Close-up of Spotweld Failure
(2 m/s, 25°, μ_c = 0.1) – Benchmark Model
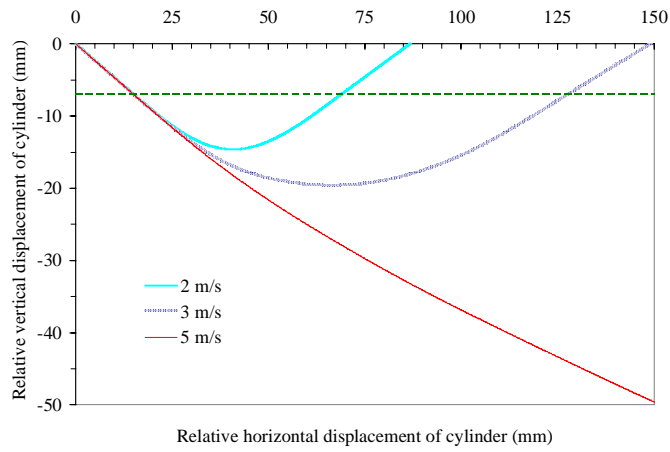
Figure 4. Comparison of Displacement Path of Cylinder into Box Beam
for Different Initial Velocities
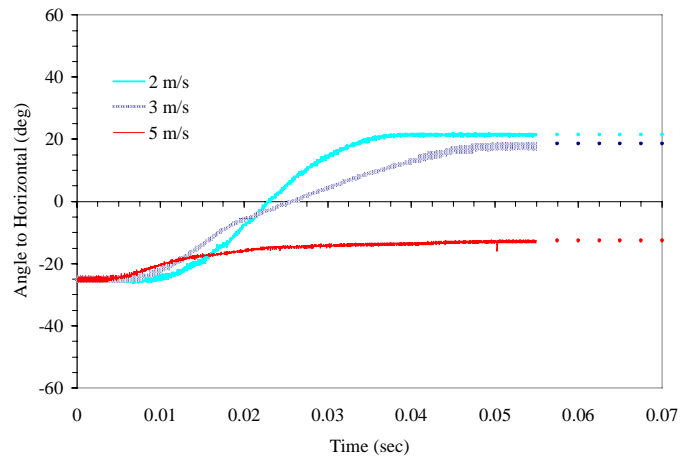
Figure 5. Comparison of Angle to Horizontal vs. Time for Different Initial Velocities
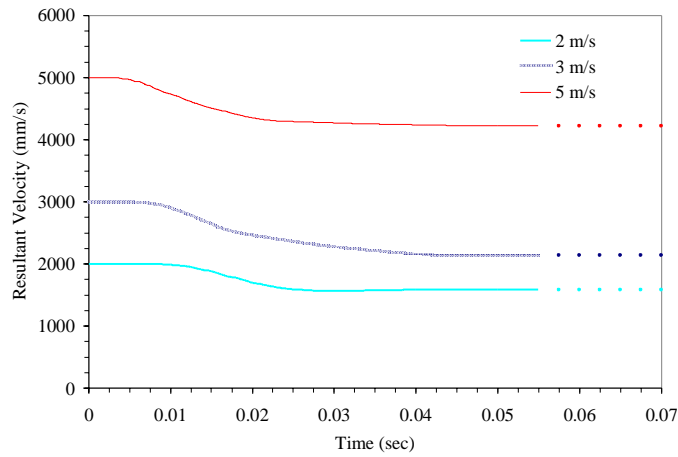
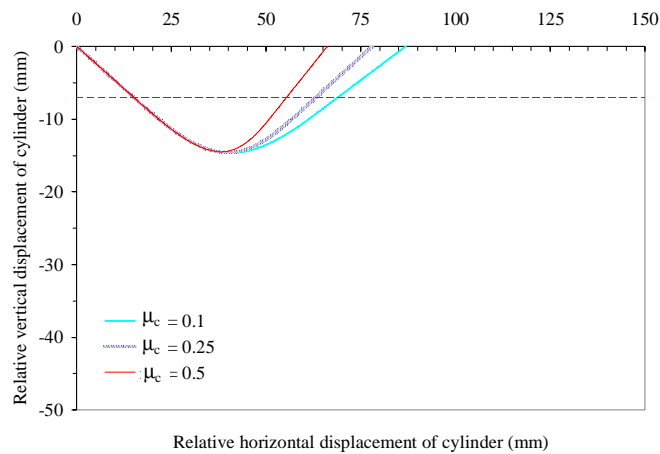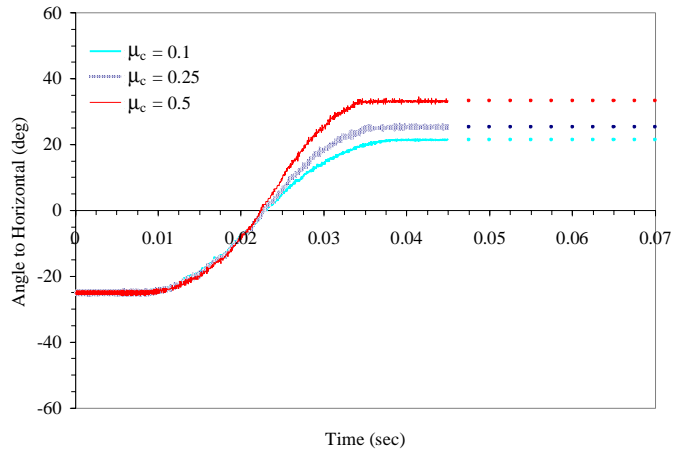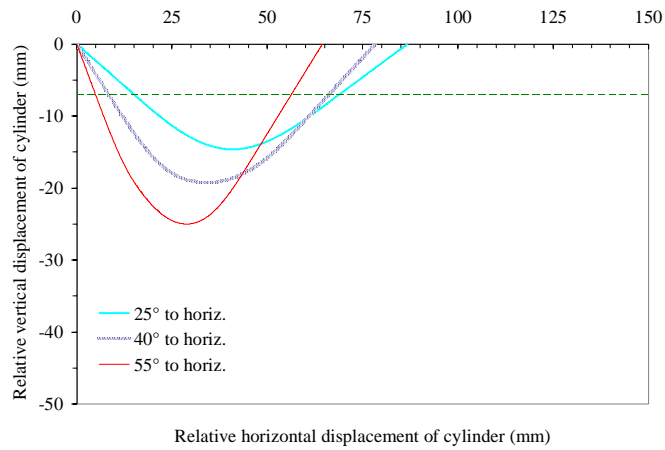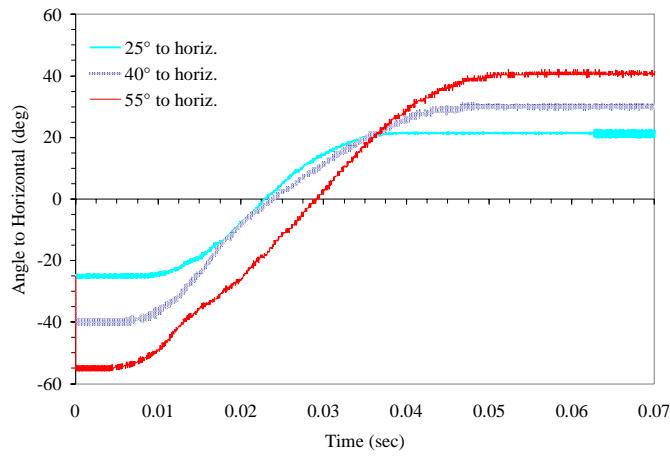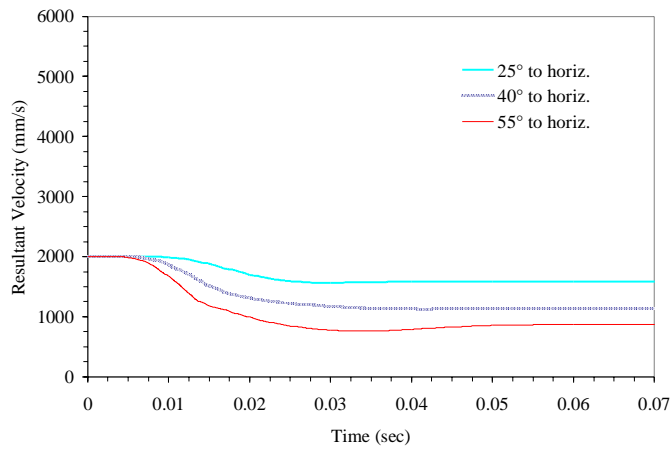Figure 6. Comparison of Resultant Velocity vs. Time for Different Initial Velocities
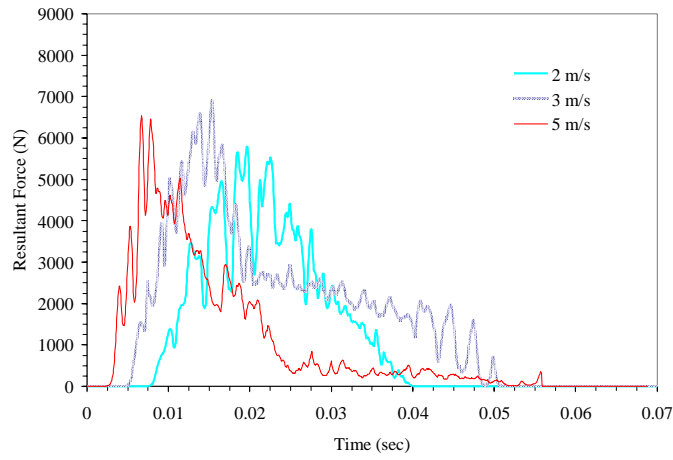
Figure 7. Comparison of Resultant Force vs. Time for Different Initial Velocities

Figure 8. Comparison of Displacement Path of Cylinder into Box Beam
for Different Functional Coefficients of Friction

Figure 9. Comparison of Angle to Horizontal vs. Time
for Different Functional Coefficients of Friction
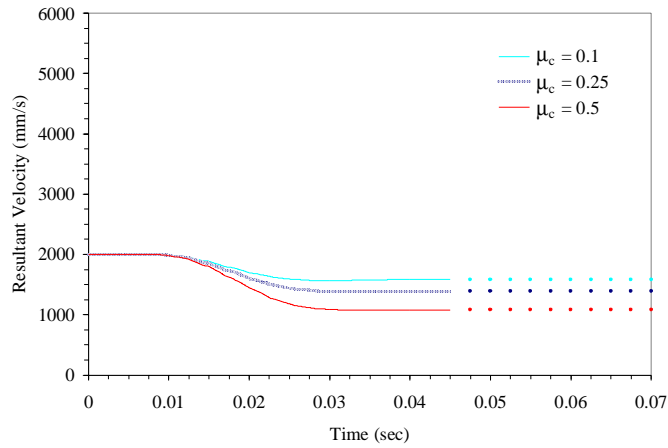
Figure 10. Comparison of Resultant Velocity vs. Time
for Different Functional Coefficients of Friction
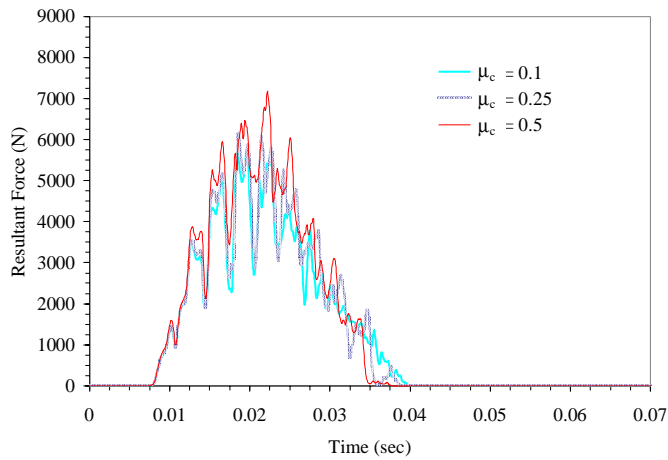
Figure 11. Comparison of Resultant Force vs. Time
for Different Functional Coefficients of Friction

Figure 12. Comparison of Displacement Path of Cylinder into Box Beam
for Different Initial Angles to Horizontal

Figure 13. Comparison of Angle to Horizontal vs. Time
for Different Initial Angles to Horizontal

Figure 14. Comparison of Resultant Velocity vs. Time
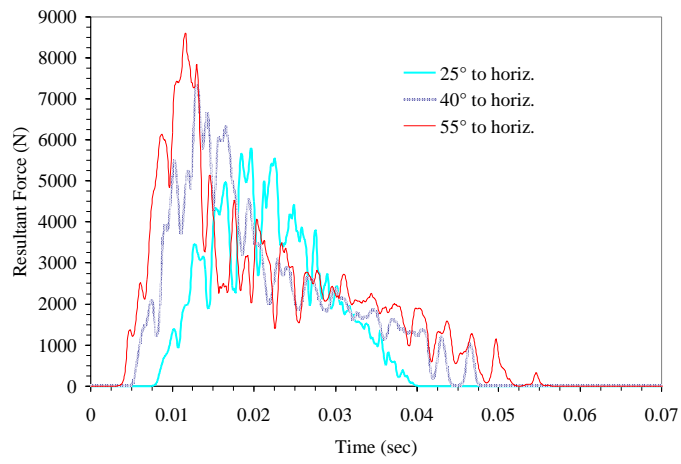for Different Initial Angles to Horizontal

11-13

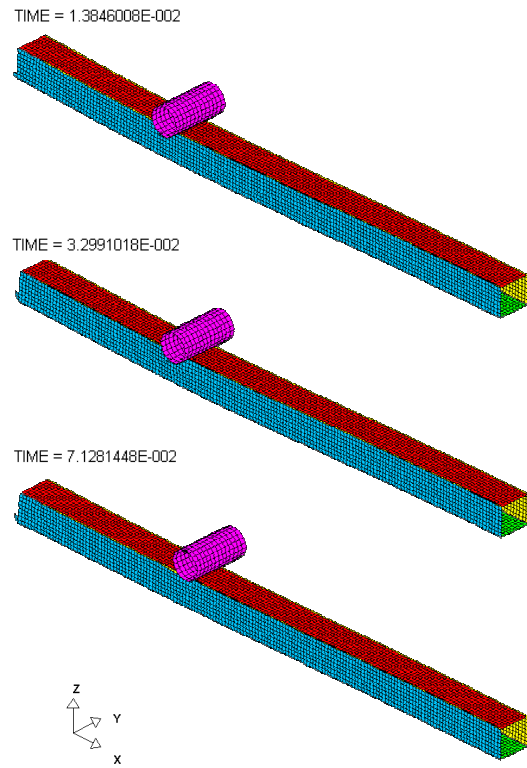Figure 15. Comparison of Resultant Force vs. Time for Different Initial Angles to Horizontal

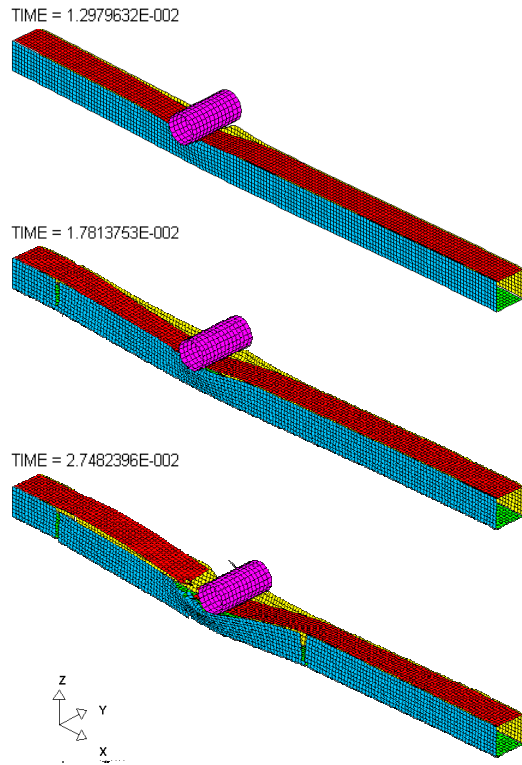Figure 16. Displacement Animation Plots (2 m/s, 55°, $\mu_c = 0.1$)

TIME = 1.2979632E-002

TIME = 1.7813753E-002

TIME = 2.7482396E-002

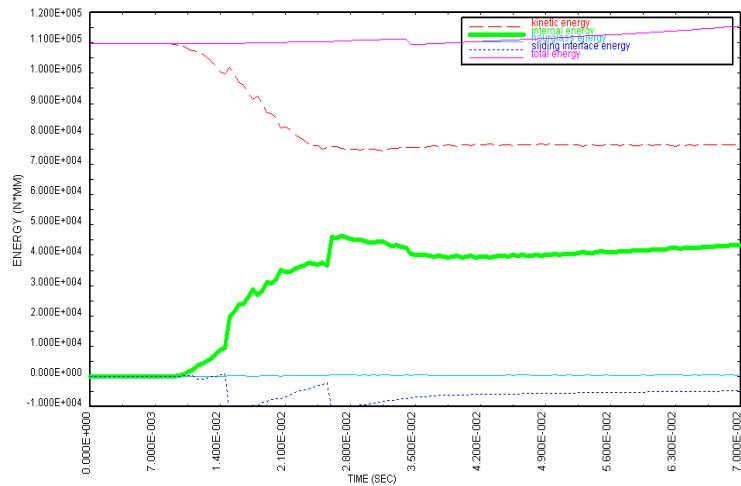Figure 17. Displacement Animation Plots (5 m/s, 25°, μ_c = 0.1)

Figure 18. Global Energy Data
(2 m/s, 25°, μ_c = 0.1) – Benchmark Model